Seismic anisotropy of the upper mantle below the Western rift, East Africa

G. Tepp[1]*, C. J. Ebinger[2], H. Zal[3], R. Gallacher[2,4], N. Accardo[5], D. J. Shillington[5], J. Gaherty[5], D. Keir[4], A. A. Nyblade[6], G. J. Mbogoni[7], P. R. N. Chindandali[8], R. Ferdinand-Wambura[9], G. D. Mulibo[9], G. Kamihanda[7]

[1] Department of Physics & Astronomy, University of Rochester, Rochester, NY, USA.

[2] Department of Earth and Environmental Sciences, Tulane University, New Orleans, LA, USA.

[3] Victoria University of Wellington, New Zealand.

[4] National Oceanography Centre Southampton, University of Southampton, Southampton, UK.

[5] Lamont-Doherty Earth Observatory of Columbia University, Palisades, New York, USA.

[6] Department of Geosciences, The Pennsylvania State University, State College, PA, USA.

[7] Geological Survey of Tanzania, Dodoma, Tanzania.

[8] Geological Survey of Malawi, Zomba, Malawi.

[9] University of Dar-es-Salaam, Dar-es-Salaam, Tanzania.

Corresponding author: Gabrielle Tepp (gtepp@usgs.gov)

* Now at Alaska Volcano Observatory, US Geological Survey, Anchorage, AK, USA.

Key Points:

- Splitting rotates from regional NE direction in south to rift parallel at Rungwe Volcanic Province
- SKS-splitting patterns are consistent with asthenospheric flow around cratonic roots, possibly enhanced by oriented melt pockets
- The long-lived, small volume Rungwe Volcanic Province may have formed above a stagnation point in asthenospheric flow between two cratons

This article has been accepted for publication and undergone full peer review but has not been through the copyediting, typesetting, pagination and proofreading process which may lead to differences between this version and the Version of Record. Please cite this article as doi: 10.1029/2017JB015409

Abstract

Although the East African rift system formed in cratonic lithosphere above a large-scale mantle upwelling, some sectors have voluminous magmatism while others have isolated, small-volume eruptive centers. We conduct teleseismic shear wave splitting analyses on data from 5 lake-bottom seismometers and 67 land stations in the Tanganyika-Rukwa-Malawi rift zone, including the Rungwe Volcanic Province (RVP), and from 5 seismometers in the Kivu rift and Virunga Volcanic Province (VVP), to evaluate rift-perpendicular strain, rift-parallel melt intrusion, and regional flow models for seismic anisotropy patterns beneath the largely amagmatic Western rift. Observations from 684 SKS and 305 SKKS phases reveal consistent patterns. Within the Malawi rift south of the RVP, fast splitting directions are oriented northeast with average delays of ~1 s. Directions rotate to N-S and NNW north of the volcanic province within the reactivated Mesozoic Rukwa and southern Tanganyika rifts. Delay times are largest (~1.25 s) within the VVP. Our work combined with earlier studies shows that SKS-splitting is rift parallel within Western rift magmatic provinces, with a larger percentage of null measurements than in amagmatic areas. The spatial variations in direction and amount of splitting from our results and those of earlier Western rift studies suggest that mantle flow is deflected by the deeply rooted cratons. The resulting flow complexity, and likely stagnation beneath the Rungwe province, may explain the ca. 17 My of localized magmatism in the weakly stretched RVP, and it argues against interpretations of a uniform anisotropic layer caused by large-scale asthenospheric flow or passive rifting.

1 Introduction

Earth's continental plates are heterogeneous in composition, thickness, and rheology, leading to differences in their response to mantle flow as well as forces applied at their boundaries. The lithosphere-asthenosphere boundary (LAB) separates the lithosphere from the weaker upper mantle (asthenosphere), yet LAB structure and physical properties show variations between cratonic and tectonically active areas. Changes in LAB structure associated with aqueous and magmatic fluid content have also been observed [e.g., *Rychert and Shearer*, 2009; *Green et al.*, 2010].

Olivine, the primary upper mantle constituent, is strongly anisotropic, and its fast direction often aligns parallel to the plate transport direction or other sustained strain [e.g., *Hess*, 1964; *Silver and Chan*, 1991; *Kendall et al.*, 2006; *Hansen et al.*, 2014]. Simple shear strain of olivine caused by the motion of plates over the asthenosphere may lead to lattice preferred orientations (LPO) readily detectable using seismic anisotropy [e.g., *Becker et al.*, 2006; *Tommasi et al.*, 2009]. Dynamic mantle processes may also create LPO in the direction of flow [e.g., *Debayle et al.*, 2005; *Behn et al.*, 2004; *Lin et* al., 2016]. In some regions, the mantle lithosphere may also contribute to observed anisotropy through oriented melt pockets with a preferential orientation due to a sustained stress field [e.g., *Gao et al.*, 1997; *Kendall et al.*, 2006; *Holtzman and Kendall*, 2010] and to fossil strain fabrics accrued during orogenesis [e.g., *Silver and Chan*, 1991; *Savage*, 1999; *Walker et al., 2004; Tommasi et al.*, 2009]. Aligned, melt-filled cracks and/or faults in the crust may contribute a small amount of splitting, owing to the much shorter path lengths over which to accrue anisotropy [e.g., *Keir et al.*, 2006; 2011]. Thus, the direction of anisotropy can be used to discriminate between these potential sources of anisotropy, providing insight to the lithospheric structure of the study area [e.g., Yu et al., 2015].

The East African Rift System (EARS) formed above a large low-velocity zone, known as the African Superplume, that rises from the core-mantle boundary to the mantle transition zone, above which data gaps and non-uniqueness blur our knowledge of plume-lithosphere interactions [e.g., *Nyblade and Robinson*, 1994; *Bastow and Fishwick*, 2011; *Chang et al.*, 2011; *Hansen et al.*, 2012; *French and Romanowicz*, 2015]. The EARS spans most of the African continent and includes incipient seafloor spreading in the Afar triple junction zone, as well as incipient continental rifting in the Southwestern rift and southernmost Eastern rift [*Ebinger and Scholz*, 2012]. The absolute motion of the very slow moving African plate is debated, with WNW predicted by the hotspot reference model of *Gripp and Gordon* [2002] and NE predicted by no-net rotation models [e.g., *Argus et al.*, 2011; *Conrad and Behn*, 2010].

Pre-existing variations in lithospheric thickness, such as unusually thick Archaean cratons, can enhance or modify mantle flow and melt production [e.g., *Sleep et al.*, 2002]. Horizontal and vertical forces induced by the dynamic flow lead to lithospheric thinning and heating as well as melt generation, but the spatial distribution of the forces remains debated [e.g., *Stamps et al.*, 2014; *Birhanu et al*., 2016; *Kendall and Lithgow-Bertelloni*, 2016]. In some areas, the mantle plume transfers heat, magma, and volatiles to the African plate, changing its composition and structure over time [e.g., *Ebinger and Sleep*, 1998; *Bastow and Keir*, 2011; *Lee et al.*, 2016].

Although several regional and local studies establish a strong context for depth distribution and spatial variations in mantle anisotropy beneath northeastern Africa [e.g., *Ayele et al.*, 2004; *Gashawbeza et al.*, 2004; *Kendall et al.*, 2006; *Hammond et al.*, 2014], anisotropy patterns in the weakly magmatic Western rift sector of the EARS are only loosely constrained by widely spaced arrays in the region [*Walker et al.*, 2004; *Bagley and Nyblade*, 2013; *Yu et al.*, 2015], a high resolution rift transect in the southern Malawi rift [*Reed et al.*,

2017], and by a dense array in southwestern Uganda [*Homuth et al.*, 2016]. We analyze seismic anisotropy patterns beneath the southern Tanganyika, Rukwa, and northern Malawi rift zones using two independent temporary seismic arrays, SEGMeNT [*Shillington et al.*, 2016] and TANGA14 [*Hodgson et al*., 2017] (Figures 2, S1, & S2). The SEGMeNT array includes the first splitting data from five broadband lake-bottom seismometers. The two networks enclose one of the few isolated volcanic provinces in the Western rift, the ca. 17 Ma-Present Rungwe volcanic province (Figures 1 & 2). We also analyze data from five stations from a temporary array in the Kivu rift and ca. 12 Ma-Present Virunga volcanic province (VVP; Figure 3). By combining these networks, the study region includes the edge of the deeply-rooted Archaean Tanzania craton, Proterozoic and Pan-African orogens, and areas affected by rifting in Permian-Cretaceous time (Figure 1). This allows for comparison of anisotropy beneath lithosphere of varying age, composition and thickness. Our objectives are to compare and contrast SKS (and SKKS) splitting patterns across ancient orogens and rift zones to evaluate the influence of fossil lithospheric fabrics and asthenospheric flow, with or without the presence of aligned melt on the orientation and magnitude of observed anisotropy.

2 Tectonic Setting

The EARS transects much of the African continent, and it traverses Archaean to Proterozoic lithosphere that experienced widespread rifting in Permo-Triassic time (Karroo) and more localized rifting in Cretaceous-Paleogene time [e.g., *McConnell et al.*, 1967; *Ebinger et al.*, 1989; *Versfelt and Rosendahl*, 1989; *De Waele et al.*, 2006] (Figure 1). The Western rift system formed in Proterozoic orogenic belts between the deeply-keeled Tanzania craton to the east and the Congo and Bangweulu cratons to the west (Figures 1 & 2). *Fishwick and Bastow* [2011] estimate lithospheric thickness from surface-wave shear-velocity imaging in Africa and indicate that the Congo and Bangweulu cratons are >160-220

km thick, relative to 120-150 km-thick lithosphere beneath the Western rift. Using body-wave and surface-wave imaging, *Ritsema et al.* [1998], *Weeraratne et al.* [2003], and *Mulibo and Nyblade* [2013] determine lithospheric thickness of ca. 200 km beneath the central Tanzania craton. These lithospheric thickness values are consistent with estimates based on independent shear wave analyses [*Fishwick and Bastow,* 2011; *O'Donnell et al.*, 2013].

2.1 Tanganyika-Rukwa-Malawi rift zone

The Proterozoic lithosphere between the cratons shows a variety of regional strain fabrics and structural orientations, ranging from NNW to NW in the Tanganyika-Rukwa area, to east-west along the southern boundary of the Tanzania craton, to N-S in the Mozambiqan (Pan-African) orogenic belt west and east of the Malawi rift [e.g., *Fritz et al.*, 2013] (Fig. 2). Much of this sector was affected by Permo-Triassic (Karroo) rifting, and sedimentary strata are preserved in basins bounded by NNE- and NE-striking normal faults (Figure 1). The exception is the NW-striking Rukwa rift between the Tanganyika and Malawi rifts; it contains up to 10 km of Karoo, Cretaceous, Oligocene and Late Miocene-Recent strata [e.g., *Morley et al.*, 1992; *van der Beek et al.*, 1998; *Hilbert-Wolf et al.*, 2016].

Our focus is the southern sector of the Western rift that includes the Tanganyika, Rukwa, and northern Malawi rift zones, all of which lie on the broad uplifted East African plateau (Fig. 1). There is no surface evidence for Cenozoic magmatism in these rift zones, except in the Rungwe volcanic province. Magmatism in the Rungwe region initiated by ca. 17 Ma [*Rasskazov et al.*, 2003; *Mesko et al.*, 2014], but much of the present-day fault architecture developed after about 8 Ma [e.g., *Ebinger et al.*, 1989; *Morley et al.*, 1992]. In the multiply-reactivated Rukwa region, however, carbonatitic ash in sedimentary strata indicate a phase of faulting and magmatism at about 24 Ma [*Roberts et al.*, 2012]. Lavas of the Rungwe volcanic province were erupted along the present-day location of large offset fault systems along the Malawi and Rukwa basins [e.g., *Ebinger et al.*, 1989].

The extension direction, determined from earthquake focal mechanisms from Global Centroid Moment Tensors, is nearly E-W in the study area [e.g., *Delvaux and Barth*, 2010; *Biggs et al.*, 2010]. Geodetic constraints are very coarse but also indicate a sub E-W extension direction [*Saria et al.*, 2014]. Extensional strains associated with Miocene-Recent rifting are, therefore, predicted to be oriented E-W but could be weak given the small amounts of stretching that have occurred in these early stage rift zones. Dikes and filled cracks are oriented NNW-SSE in the Rungwe province [e.g., Ebinger et al., 1989; Fontijn et al., 2010]. Normal faults beneath Lakes Tanganyika and Malawi where structures are well imaged by seismic reflection data also strike N-S to NNW [e.g., *Ebinger et al.*, 1989; *Rosendahl et al.*, 1992; *Mortimer et al.*, 2007; *McCartney and Scholz*, 2016]. Mesozoic faults strike NNE to NE throughout the region, excluding the NW-trending Rukwa rift zone [e.g., *Castaing*, 1991; *Ring et al.*, 1994].

Estimates of crustal stretching from basin modeling and fault reconstructions are 10-20%, decreasing to <10% in the southern Malawi rift [*Morley et al.*, 1992; *Ebinger et al.*, 1991]. However, results from receiver function studies suggest that these are underestimates. They indicate that crust thins from about 41 km on the rift flanks to 27 km beneath the fault bounded southern Tanganyika basins, or ≤ 32% extension [*Hodgson et al.*, 2017]. Receiver functions from the northern and central basins of the Malawi rift indicate thinning from ~44 km to 33 km, or ~25% extension [*Borrego*, 2016]. Surface-wave tomography indicates that lithospheric thinning is greatest beneath the Rungwe volcanic province, and results suggest that the zone of mantle lithospheric thinning and heating is 50-100 km broader than the width of the fault-bounded basins [*Accardo et al.*, 2017]. Extensional strains associated with Miocene-Recent rifting are, therefore, predicted to be weak and oriented E-W.

2.2 Kivu rift

The Kivu rift is part of the Albertine Rift, the northern sector of the Western rift (Figure 3) and last deformed during the Phanerozoic [e.g., *Fernandez-Alonso et al*., 1998]. Geochemical and geophysical data suggest that mantle plume processes contribute to regional uplift at a variety of length scales [*Ebinger et al.,* 1989; *Chakrabarti et al.,* 2009]. The NE-trending Mesoproterozoic Kibaran Belt lies to the west of the Tanzanian craton and east of Lake Kivu (Figure 3). The northeastern part of the Kivu rift comprises N-S trending structures, whereas crustal structures in the southern part of the rift are NW-trending [*Wood et al.,* 2017; *Smets et al.,* 2016]. The Kivu rift comprises two major basins bounded on one or both sides by large offset border fault systems (Fig. 3). Magmatism has affected the Kivu rift zone since at least 12 Ma when lavas at the base of the Virunga province were erupted [*Kampunzu et al.,* 1998]. Large parts of the North Kivu basin are covered by extensive lava flows of the Virunga volcanic province, including Nyiragongo and Nyamuragira, two of the most active volcanoes in Africa [*Smets et al.,* 2016; *Wood et al.,* 2017].

The crustal thickness beneath the Kivu rift is estimated, by seismic refraction experiments, to be ~30 km [*Bram and Schmeling*, 1975]. Crust beneath the Virunga province is heavily intruded with high upper crustal velocities interpreted as a thick basalt sequence above a mid-crustal low-velocity zone [*Mavonga et al.*, 2010]. Teleseismic S to P conversions at the velocity discontinuity at the base of the lithosphere indicate two distinct discontinuities at 50-100 km and 140-200 km beneath the Edward and Albert basins, the next segment north of the Kivu rift [*Wölbern et al.*, 2012]. The upper velocity discontinuity is interpreted to represent the upper boundary of melt infiltrated and metasomatized lithosphere, whereas the lower discontinuity is interpreted to represent the lithosphere-asthenosphere boundary [*Wölbern et al.,* 2012].

3 Data and Methods

Shear-wave splitting of teleseismic body-waves (e.g., SKS, SKKS) can be used to measure anisotropy of the upper mantle [e.g., *Savage*, 1999]. A polarized shear-wave traveling through an anisotropic material will split into orthogonal waves, with one polarization traveling faster than the other. The measured polarization of the split waves (fast splitting direction, ϕ) gives insight into the orientation of the anisotropic axes. The difference in the arrival time between the split waves (the delay time, δt) is affected by the strength of the anisotropy and the distance traveled through the anisotropic layer. For teleseismic body-waves with near vertical incident angles (< ~15°), the distance traveled through the anisotropic layer will be close to the thickness of the layer. SKS and SKKS phases convert from a P-wave to an S-wave at the core-mantle boundary. Upon conversion, the S-wave becomes radially polarized losing all information about anisotropy along its previous path and, thus, retaining only anisotropic effects from its path between the core-mantle boundary and the receiver.

We use 48 teleseismic earthquakes of $M_W \geq 6.45$ at distances between 85º-130º that were recorded on the SEGMeNT temporary array between August 16, 2013 and September 24, 2015, 64 teleseisms of $M_W \geq 5.55$ at distances between 90º-130º that were recorded on the TANGA14 temporary array between June 24, 2014 and August 23, 2015, and 46 teleseisms of $M_W \geq 5.5$ at distances between 90º-140º that were recorded on the KIVU12 temporary array between March 17, 2012 and April 7, 2013 (Figure 4c). Lake-bottom seismometer (LBS) data from the Malawi rift (Lake Malawi/Nyasa) were acquired as part of the SEGMeNT experiment between March 3, 2015 and October 25, 2015 and include 14 teleseisms of $M_W \geq 6.25$ at distances between 90º-130º. Distances for all measured earthquake-station pairs are shown in Figure 4a. For the SEGMeNT array, 15 stations in Tanzania began recording at the starting date in August 2013 with an additional 25 stations in

Tanzania and 15 stations in Malawi beginning in July 2014 (Figures 2 & S1). One of the Tanzania stations (TIRI) had poor horizontal component recordings and was excluded from our analysis. The IRIS-PASSCAL broad-band sensors included Trillium 40, Guralp CMG-3T, and Streckeisen STS-2. The TANGA14 array (Figures 2 & S2) comprised 3 Guralp ESP and 10 Guralp 6TD stations from the SEIS-UK pool that were deployed in Tanzania. From the Kivu experiment, we used 5 IRIS-PASSCAL broad-band seismometers, Trillium 120 and Guralp CMG-40T, located in Rwanda (Figure 3). Three other Kivu seismometers had locked channels and could not be used in this study.

We used the SplitLab software for MATLAB [*Wüstefeld et al.,* 2008] to measure SKS and SKKS splitting. Before making the measurements, the waveforms were rotated into the LQT coordinate system with the L-component in the longitudinal direction, the Q-component in the radial direction, and the T-component orthogonal to L and Q. A range of filters were then applied to maximize the signal-to-noise ratio, and a time window was chosen around the desired phase. The time window was chosen to be as large as possible and be stable over a minimum of three different time windows. Finally, the splitting measurements were made with two different methods. The rotation correlation (RC) method [e.g., *Bowman and Ando,* 1987] uses a grid search to determine the rotation angle and time delay that maximizes the cross-correlation coefficient between the uncorrected Q- and T-components. The second method (SC), developed by *Silver and Chan* [1991], works by minimizing the T-component energy which should be zero for waves with an initial radial polarization. Null measurements were determined by the initial linearity of the particle motion and the lack of signal on the T-component. Each measurement was given a quality rating of good, fair, or poor that was based on the initial ellipticity of the particle motion, the linearity of the corrected particle motion, the waveform quality, the similarity of the fast and slow split shear waveforms, and the agreement between the RC and SC methods [e.g., *Barruol et al.*, 1997].

We used varying bandpass filters to maximize the number of measurements made from our limited dataset. The noise levels and primary signal frequency are variable from station-to-station and teleseism-to-teleseism; thus, varying the filter limits allowed us to more easily identify the signal. Filters used a lower bound between 0.01-0.05 Hz and an upper bound between 0.09-1 Hz. The average filter bounds were 0.018 and 0.36 Hz for SKS and 0.019 and 0.34 Hz for SKKS. *Barruol and Ismail* [2001] used varied filters and found no evidence for frequency dependent anisotropy, but they did find that narrower filter bands resulted in higher errors. Thus, we used wider filter bands when possible.

3.1 Limitations and Sources of Error

Both the RC and SC methods assume an initial radial polarization equal to the back-azimuth (measured clockwise from north) [*Wüstefeld et al.*, 2008]. In this study, teleseism back-azimuths primarily clustered around the east and west directions with few-to-none in the north or south directions (Figure 4b). Sensor misorientation and deviations from the assumed polarization potentially add uncertainty to the splitting measurements; the SC method results are particularly sensitive to these rotation errors. This sensitivity could be a consequence of SplitLab's implementation of the method, rather than the method itself; however, *Yu et al.* [2015] also found a large sensitivity to sensor misorientation using the *Liu and Gao* [2013] implementation of the SC method. Thus, we applied misorientation corrections when possible to minimize rotation errors. For the SEGMeNT stations, sensor orientations (Table S1) were estimated from analyses of teleseismic arrivals and from ambient noise, with values from the two methods generally showing very good agreement, particularly for the shorter time period LBS data [*Accardo et al.*, 2017]. TANGA14 station orientations were re-measured at retrieval, and corrections were made with these values. Empirically-determined corrections were applied to 2 of the Kivu stations (Table S1). These corrections improved the agreement of the RC and SC methods.

The signal-to-noise ratio (SNR) was calculated by the procedure of *Restivo and Helffrich* [1999]. This procedure calculates SNR in the measurement window after the splitting correction is made using the Q-component as the signal and the T-component as the noise. Because SNR is calculated after the splitting correction is made, it must be calculated separately for each method. On average, the SNR for SC measurements is higher than that for the RC measurements. This is a consequence of how the different methods correct for splitting. Because the SC method minimizes energy on the T, the assumed noise (i.e., T-component) would likely be lower amplitude than for the RC method, leading to higher SNR for SC measurements. Table S2 provides a summary of the minimum, maximum, and average SNR at each station. Figures S3-S6 show examples of low and high SNR measurements for a land-based station and an LBS.

Restivo and Helffrich [1999] found that SC anisotropy measurements with SNR > 8 were valid for any back-azimuth polarization, whereas measurements with 4 < SNR < 8 were only reliable for waves with back-azimuths >20° from the fast splitting direction. Over 94% of all measurements had SNR > 4 for both methods. For SKS, 54% of RC measurements and 67% of SC measurements had SNR > 8. These percentages decrease to 36% and 53% for SKKS RC and SC measurements, respectively. Many of the earthquakes used in this study have back-azimuths similar to the measured splitting directions, so it is important that at least 54% of all SKS measurements are reliable with no further checks on the data. SNR averages for each array are listed in Table 1.

4 Results

In total, we made 684 SKS measurements and 305 SKKS measurements on 77 total stations for an average of 8.8 SKS and 3.9 SKKS measurements per station. The number of measurements at a given station ranged from 1-27 for SKS and 0-21 for SKKS. The average error for ϕ was 19.4° for RC SKS, 23.5° for SC SKS, 21.7° for RC SKKS, and 25.1° for SC

SKKS. For δt, the average error was 0.36 sec and 0.63 sec for RC and SC SKS, respectively, and 0.49 sec and 0.73 sec for RC and SC SKKS, respectively. For individual measurements, the RC method typically provides a lower δt error but a slightly higher error in ϕ. The measurement numbers and error results for each array are listed in Table 1.

All measurements are plotted in Figure 5 for SEGMeNT and TANGA14 arrays and Figure S7 for the Kivu array as the surface projection of the location where the seismic rays cross the base of the lithosphere (pierce point), estimated at about 200 km subsurface. Figure S8 shows the measurements plotted at the 100 km pierce points, within the lithosphere, except perhaps beneath the RVP and KVP. The RC method tends to have more consistent results, while the SC method shows more variation. This is likely a consequence of the sensor misorientation effects on the SC method described in Section 3.1. Adding an empirically determined sensor orientation correction showed a convergence between the RC and SC results, with the resultant splitting parameters more similar to the original RC results. Thus, the RC method results appear more robust and are presented here.

The back-azimuths of null measurements are approximately perpendicular or parallel to measured fast splitting directions (ϕ, measured clockwise from north; Figure 5). Null measurements can occur from 1) alignment with the fast or slow splitting direction, 2) multiple anisotropic layers that cancel each other out, or 3) lack of anisotropy. Our null measurements are consistent with the first interpretation on most stations (Figure 5), where non-nulls are also detected (Figures S9 to S12). There are a few stations with only null measurements: 4 stations for SKS and 16 stations for SKKS. However, the back-azimuths at the null-only stations are generally parallel or perpendicular to splitting directions at adjacent stations.

Results at each station were circularly averaged [e.g., *Mardia*, 1975] with the measurements weighted by their quality rating (described in section 2): good = 3, fair = 2,

and poor = 1 (Figures 6 & 7 and Table S3). We also calculated a weighted circular standard deviation at each station. Although several stations have very few SKKS picks and may be misleading, the SKKS results are reasonably similar to the SKS results (Figure 8). Splitting from aligned olivine crystals is strongest on vertically propagating shear waves [*Kendall et al.*, 2006], so steeper incident angles should show greater sensitivity to mantle anisotropy. The SKS phases have more vertical incident angles than the SKKS phases and should sample a smaller lateral area of the anisotropic layer (i.e., fewer horizontal variations) in addition to being more strongly affected by the anisotropy. Another possibility for the difference is multiple layers of anisotropy that affect the splitting magnitude in different ways or the addition of anisotropy accrued in the lower mantle [e.g., *Lynner and Long*, 2014]. As independent analyses of surface wave anisotropy from SEGMeNT and Tanganyika data become available, we can evaluate the depth distribution of the anisotropy and models for the null results. In this study, we will focus on analyzing the SKS results. Additionally, average splitting results for back-azimuths from 0-180° (eastern directions) and 180-360° (western directions) are largely similar with only minor differences.

The splitting results can be summarized in four broad areas: the Kivu rift (KIVU12), the Tanganyika –Rukwa trough west of 32.5°E (TANGA14), and east and west of the Malawi rift axis at 34.3°E (east and west SEGMeNT). The area east of the Malawi rift has the most consistent splitting direction: all but one land station and one LBS have NE splitting, with observed SKS splitting directions of $21° < \phi < 56°$ and delay times of $0.46 \text{ sec} < \delta t < 1.29 \text{ sec}$ (Figure 8). West of the Malawi rift, the area south of -10.3°N also has a NE- splitting direction ($34° < \phi < 52°$) but with slightly smaller delay times on average ($0.47 \text{ sec} < \delta t < 0.93 \text{ sec}$). Moving north in the west SEGMeNT array, the splitting direction largely rotates to the NW, except for the RVP which includes stations with wide variations in splitting and relatively high percentages of null measurements, including one null-only station (Figures 6,

8, and S9). The western flank of the North basin RVP includes two null-only stations and has stations with some of the largest discrepancies between the RC and SC methods. North of the RVP (-8.9°N), the splitting directions are -102° (78°) < ϕ < -39° with delay times of 0.75 sec < δt < 1.21 sec that are similar to the region east of the Malawi rift. In the Tanganyika-Rukwa region, stations on the western side of the Rukwa rift largely show NW splitting directions with the northernmost station having N-S splitting. Stations on the eastern side of the Tanganyika rift show a mix of NW and NE splitting directions and high percentages of null measurements (most stations >70%; Table S3, Figure S9).

The Kivu rift area has the largest splitting with a weighted average δt of 1.24 sec. The two stations (KV05, KV07) west of Karisimbi volcano have nearly N-S splitting parallel to rift faults and dike intrusions, whereas the station south of Karisimbi (KV08) has a NE splitting direction, and the largest percentage (41%) of nulls for this array. The only site outside the volcanic province, KV01, has a NW splitting direction (Figures 6 and 8). KV06, on the flank of NW-striking rift fault, has only null measurements (Figure S11).

5 Discussion

The detail afforded by these dense networks allows us to evaluate the relative contributions of 1) fossil lithospheric strain fabrics, 2) rift-related extensional strain fabric, 3) absolute plate motions, 4) oriented melt pockets, and 5) dynamic mantle flow patterns to the observed SKS splitting measurements.

5.1 Fossil strain fabric

Laboratory measurements demonstrate that pervasive strain fabrics in the crust and mantle lithosphere may result in detectable anisotropy [e.g., *Tommasi et al.*, 2009]. As discussed in 5.3, the metamorphic fabric and orientation of shear zones near the cratons shows parallelism with their surface contacts, indicating that the geometry of the cratons themselves influenced Proterozoic lithospheric deformation. The ϕ and δt patterns also show

some parallelism and rotation near the craton boundaries, which may be the combined effect of fossil lithospheric fabric and modern mantle flow (Section 5.3).

Splitting patterns away from the Tanzania and Bangweulu craton boundaries show no clear parallelism with tectonic fabric, particularly within the Ubendian belt east of Lake Malawi (Nyasa). Although sections of the Livingstone fault system bounding the North basin reactivate NW-striking Proterozoic mylonites, ϕ shows a NE orientation. Along the Tanganyika rift flanks, splitting parallels shear zones within the narrow Ubendian orogenic belt, but the amount of splitting is small in comparison to the NE fabric south of the RVP. Splitting at some stations in the Irumides belt parallel the NE-shear zone fabric, but the splitting direction and delays rotate to NW or become null to the north (e.g., Fig. 2). The increase in nulls with the rotation may indicate a combination of sources [e.g., *Saltzer et al.,* 2000], but the time series of observations is too short to enable fuller evaluations. Splitting directions in the area of convergence between the NW-trending shear zones of the Ubendian belt, the NE-SW trending structures of the Irumides belt, the Bangweulu block to the northwest, and the Luangwa graben to the southeast are highly oblique to the metamorphic fabrics. The regionally occurring NE splitting direction is perpendicular to the inferred extensional strain fabric during Karroo rifting, arguing against a rift-induced strain fabric. Although local variations exist, the NE-splitting direction seen throughout the Malawi rift south of the RVP suggests contributions from modern tectonic or mantle processes.

5.2 Rift-related extensional strain fabric

A second possible contribution to the observed anisotropy is a rift-perpendicular strain fabric [e.g., *Eilon et al.,* 2014]. Although the NE splitting direction is sub-parallel to the Malawi rift opening direction, the delay times are smaller within the rift basin where crustal strain is largest [*Borrego,* 2016; *Accardo et al.,* 2017] than on the rift flanks 100 km from the nearest fault. For example, splitting patterns determined from lake bottom seismometers

show both the dominant NE orientation, as well as a NNW to N-S splitting direction parallel to major faults within the basin (Fig. 6). The Rukwa rift zone shows little evidence for an extensional strain fabric, yet it has been extended in a NE-direction during both Karroo and recent rifting. And, in the faulted Tanganyika rift basins, splitting directions are largely rift parallel. Two of the stations with NE splitting directions only have 1 non-null measurement, while the other two have high weighted standard deviations, indicating that a wide variety of splitting directions were observed at those stations. Only one of 5 sites in the Kivu rift is parallel to extension direction (KV05). Based on the combined networks and earlier data sets, we find little evidence that the East African rift imparts a significant rift perpendicular strain fabric.

5.3 Absolute plate motion and mantle flow

The consistent NE splitting direction in this region matches the general NE trend seen throughout East Africa (Figure 9), which *Yu et al.*, [2015] and *Reed et al.* [2017] attribute to LPO developed in response to absolute plate motion predicted from no-net rotation plate models [*Conrad and Behn*, 2010; *Argus et al.*, 2011].

NE-directed mantle flow from the African superplume, which rises beneath southern Africa, may enhance the regional NE-directed flow, if the asthenospheric flow is faster than the slow-moving plate [e.g., *Fishwick and Bastow*, 2011; *Bagley and Nyblade*, 2013]. Mantle flow may deviate around the edges of the thicker Bangweulu block, and create both margin parallel and perpendicular fabrics, large delay times, and upward-directed flow [e.g., *Fouch et al.*, 2000; *Sleep et al.*, 2002; *Currie and van Wijk*, 2016]. This agrees well with the observations of delay times of ~1 s and boundary parallel splitting along the eastern boundary of the Bangweulu craton, as well as null measurements within the RVP (Figs. 6 & 7). The < 200 km-wide zone of thinned lithosphere between the Bangweulu block and Tanzania craton

additionally may channel asthenospheric flow NW, explaining at least in part the rotation from the NE to NW splitting directions.

The dense splitting measurements in the northern Malawi rift reveal the rotation of splitting directions from NE in the south to NW, with the RVP at the turning point (Figure 8). Between stations in the RVP and the southern NE-splitting stations, the stations show a rotation of ϕ to NW and include two stations with only null measurements. The northernmost stations, however, continue the rotation trend and show primarily NW to NNW splitting. When taken as a whole, the observed rotation in splitting directions coincides with the edges of the Tanzania craton to the north and the Bangweulu craton to the west. Previous studies have detected a rotation of ϕ to parallel the perimeter of the Tanzania craton that was attributed to mantle flow deflected by the deeper cratonic keel [e.g., *Walker et al.*, 2004; *Bagley and Nyblade*, 2013]. The detail afforded by the combined SEGMeNT and TANG14 arrays observed rotations south of the craton from the NE direction observed throughout southern and central Africa [e.g., Reed et al., 2017], consistent with mantle flow deflected by the Tanzania craton. Predicted SKS splitting from modeling of a plume impinging on a cratonic root in a similar setting [*Sleep et al.* 2002] shows a pattern of significant changes in anisotropy direction over a very short distance, similar to that observed in this study.

Where the mantle flow impinges on the Tanzania craton and diverts around it, a stagnation point could form (Figure 10). This stagnation, along with the possible upward flow from beneath the Bangweulu craton, could promote melt generation beneath the RVP [e.g., *Ebinger and Sleep*, 1998; *Holtzman and Kendall*, 2010] and potentially explain the 17 My of magmatism with only minor extension in the RVP. The large number of null measurements in this region lends more support for local areas of flow stagnation.

5.4 Oriented Melt Pockets

Aligned melt bodies and fluid-filled cracks in the lithosphere beneath rift zones can produce rift-parallel crust and mantle splitting patterns, such as in the Ethiopian and Eastern rifts and the northern sector of the Western rift [e.g., *Gao et al.*, 1997; *Barruol and Ismail, 2001*; *Holtzman and Kendall, 2010; Keir et al., 2011; Albaric et al., 2014; Homuth et al., 2016*] (Figure 9). Although there is little evidence for rift-parallel anisotropy south of the RVP, earlier studies in the weakly magmatic Ugandan rift sector reveal rift-parallel anisotropy [*Homuth et al.*, 2016] (Figure 9). As outlined below, our results also show the same correlation between rift-parallel anisotropy and magmatism.

Holocene Plinian eruptions at Rungwe volcano and an historic eruption at Kiejo volcano within the RVP indicate active magma reservoirs beneath at least two of the volcanoes [e.g., *Fontijn et al.*, 2012]. Stations nearest Kiejo and Rungwe volcanoes have only null measurements (MZUN, IGOM). Several stations along the edge of the RVP show null splitting measurements, indicating complex layering or sub-vertical strain fabrics. Although there is no surface expression of magmatism in the Tanganyika rift, *Hodgson et al.* [2017] determine high crustal v_P/v_S ratios from receiver function analyses and interpret new results and existing data as evidence for active magmatism in the lower crust beneath the southern Tanganyika rift. From ambient noise tomography, the lowest shear wave velocities in the upper mantle occur beneath the RVP and southern Rukwa rift, but they do not continue beneath the Malawi rift [*Accardo et al.*, 2017]. *O'Donnell et al.* [2013] also find low Pn and Sn beneath the RVP and Rukwa rift region, but they do not extend beneath the Malawi and Tanganyika rifts. These independent studies argue against significant heating and melt production outside the RVP. Vertically oriented melt pockets within the extending lithosphere can, therefore, explain null SKS-splitting patterns within the Northern basin, the RVP, and the southern Tanganyika rift. The location of these magmatic provinces, in turn, may be a

consequence of enhanced vertical flow and stagnation along topography at the lithosphere-asthenosphere beneath cratonic edges.

Splitting measurements within the Kivu rift may also be affected by both horizontally and vertically oriented melt pockets. The Kivu sector has the largest delay times of all sectors, with a weighted average δt of 1.24 sec. The two stations (KV05 and KV07) between the active Nyiragongo and Nyamuragira volcanoes and the dormant Karisimbi volcano show nearly north-south splitting, while the southernmost station (KV01) has a northwest splitting direction parallel to the strong metamorphic fabric in the region. All of the stations located on volcanic strata in the Virunga volcanic province have null measurements and high standard deviations of ϕ, similar to those in the RVP sector. The NW and N-S ϕ patterns parallel the two magmatic trends: active dike intrusion from reservoirs beneath Nyiragongo strike approximately N-S [*Wauthier et al.*, 2012], whereas the aligned chain of volcanoes, faults, and fissures west of the Kivu rift strike NW [*Smets et al.,* 2016; *Wood et al.,* 2017].

Data from southwestern Uganda are highly complementary to our results, and they extend coverage northward along the Western rift. *Homuth et al.* [2016] measured SKS-splitting at 43 stations in a dense temporary network spanning parts of the Edward, Semliki, and Albert basins and focused on the Rwenzori horst (Fig 3). Fast directions parallel rift border faults and have an average delay time of about 1 s. Splitting measurements from local mantle earthquakes are nearly an order of magnitude higher than those of co-located lower crustal earthquakes, indicating that the mantle is the dominant contributor to the observed anisotropy. Finite-frequency waveform modeling show that the rift-parallel fast polarizations are consistent with horizontal transverse isotropy, interpreted as rift-parallel magmatic intrusions or lenses located within the lithospheric mantle [*Homuth et al.,* 2016].

Summarizing, our measurements reveal more variation in splitting than can be explained by either fossil fabrics [e.g., *Walker et al.*, 2004], a uniform anisotropic layer

caused by large-scale asthenospheric mantle flow [e.g., *Bagley and Nyblade*, 2013], or passive rifting within the Malawi rift sector. The inconsistent correlation of splitting directions and delay times with fossil fabrics argues against a dominant contribution from fossil strain fabrics within the crust and mantle lithosphere. We instead interpret our combined data sets as evidence for anisotropy induced by magma-filled cracks in the crust and mantle beneath the Rungwe and Virunga volcanic provinces. The northern (Tanganyika rift) and southern (Malawi rift) extent of the RVP melt intrusion into the mantle and crust remains poorly constrained, and awaits detailed analyses of crust and upper mantle velocity studies. Mantle flow from the African superplume may enhance the absolute plate motion induced anisotropy, depending on the relative velocity of the slow-moving African plate and the asthenosphere. Complexity in the flow due to interactions with the topography at the LAB, as well as contributions from fossil fabrics, can help explain the rotation in splitting directions, and perhaps the increase in null values, observed from south to north in the region and the presence of magmatism in the RVP (Figure 10).

6 Conclusions

We measured shear wave splitting parameters for the SEGMeNT, TANGA14, and KIVU12 arrays in the weakly magmatic Western rift to characterize the upper mantle anisotropy of the region and to better understand cratonic rifting processes. A total of 684 SKS and 305 SKKS splitting measurements, including the first lake-bottom seismometer measurements, were made at stations spanning four orogenic belts lying near the Tanzania and Bangweulu cratons and spanning two volumetrically small volcanic provinces (Rungwe, Virunga). The majority of stations in the Malawi rift have ϕ oriented NE and delay times of ca. 1 s, but the splitting direction rotates to NW in the northern part of the Malawi rift that encloses the Rungwe volcanic province. The largest delays (1.24 s average) are found in the Virunga volcanic province at the northern end of the Kivu rift where splitting directions are

rift-parallel. The lack of correlation between splitting directions and ancient strain fabrics or with modern extension direction argue against large contributions from LPO fabrics within the lithosphere. Oriented melt pockets may explain the rift-parallel orientations and delay times > 1 s within the Kivu and Rungwe volcanic provinces and the southern Tanganyika rift. South of the Rungwe volcanic province, ϕ direction is NE on both sides of the Malawi rift, consistent with the majority of ϕ measurements in southern Africa as compiled in *Reed et al.* [2017], and ϕ is parallel to the absolute plate motion direction from no net rotation models. The NE splitting in the Malawi rift region most likely measures mantle flow perhaps enhanced by upwelling from the super-plume originating in the lower mantle below southern Africa.

The rotation to W and NW splitting directions north of the RVP may result from deflection of the NE mantle flow by the zone of thinner lithosphere between the Archean Tanzania craton and the Bangweulu block. If upper mantle flow is directed NE, the thicker lithosphere beneath the Bangweulu block may deflect mantle flow from the Rukwa rift. Combined, the lithospheric thinning within the rift zone and the thick cratonic lithosphere may lead to a vertical component to flow and result in the generation of melt. This flow deflection by thick cratonic roots, and likely stagnation point, may explain the presence of the Rungwe Volcanic Province within an otherwise amagmatic section of the EARS. Horizontally oriented melt pockets may also contribute to the observed anisotropy in and around the volcanic provinces. Our interpretations await testing with regional flow models and better constraints on the depth extent of anisotropy from shear wave studies.

Acknowledgments and Data

We would like to thank Maureen Long and Ian Bastow for helpful advice and discussion. The field deployments would not have been possible without the efforts of the SEGMeNT and TANGA14 teams and the support of the Tanzania Geological Survey, Malawi

Geological Survey, and the University of Dar-es-Salaam. We thank two anonymous reviewers and the associate editor for helpful comments on the manuscript. This work was supported by NSF grant EAR-1109302 and funding from Beach Petroleum and Tanzania Petroleum Development Corporation. Seismic data are archived at the IRIS Data Management Center, and station-by-station results for the TANG14, KIVU12, and SEGMeNT data sets can be found in the Supporting Information.

References

Accardo, N. J., J. B. Gaherty, D. J. Shillington, C. J. Ebinger, A. A. Nyblade, G. J. Mbogoni, P. R. N. Chindandali, R. W. Ferdinand, G. D. Mulibo, G. Kamihanda, D. Keir, C. Scholz, K. Selway, J. P. O'Donnell, G. Tepp, R. Gallacher, K. Mtelela, J. Salima, and A. Mruma (2017), Surface wave imaging of the weakly extended Malawi Rift from ambient-noise and teleseismic Rayleigh waves from onshore and lake-bottom seismometers, *Geophysical Journal International*, 209(3), 1892-1905, doi: 10.1093/gji/ggx133.

Albaric, J., J. Déverchère, J. Perrot, A. Jakovlev, and A. Deschamps (2014), Deep crustal earthquakes in North Tanzania, East Africa: Interplay between tectonic and magmatic processes in an incipient rift,*Geochemistry, Geophysics, Geosystems*, *15*(2), 374-394.

Argus, D.F., R.G. Gordon, and C. DeMets (2011), Geologically current motion of 56 plates relative to the no- net- rotation reference frame, *Geochemistry, Geophysics, Geosystems*, 12(11).

Ayele, A., G. Stuart, and J. M. Kendall (2004), Insights into rifting from shear wave splitting and receiver functions: an example from Ethiopia, *Geophys. J. Int.*, 157(1), 354-362, doi: 10.1111/j.1365-246X.2004.02206.x.

Bagley, B., and A. A. Nyblade (2013), Seismic anisotropy in eastern Africa, mantle flow, and the African superplume, *Geophys. Res. Lett.*, 40, 1500–1505, doi:10.1002/grl.50315.

Barruol, G., and W. B. Ismail (2001), Upper mantle anisotropy beneath the African IRIS and Geoscope stations, *Geophys. J. Int.*, 146(2), 549-561.

Barruol, G., P. G. Silver, and A. Vauchez (1997), Seismic anisotropy in the eastern United States: Deep structure of a complex continental plate, *J. Geophys. Res.*, 102(B4), 8329–8348, doi:10.1029/96JB03800.

Biggs, J., E. Nissen, T. Craig, J. Jackson, and D.P. Robinson (2010), Breaking up the hanging wall of a rift- border fault: The 2009 Karonga earthquakes, Malawi, *Geophys. Res. Lett.*, 37(11).

Birhanu, Y., Bendick, R., Fisseha, S., Lewi, E., Floyd, M., King, R. and Reilinger, R., 2016. GPS constraints on broad scale extension in the Ethiopian Highlands and Main Ethiopian Rift. *Geophysical Research Letters*, *43*(13), pp.6844-6851.

Borrego, D., (2016), Crustal Structure of the Rungwe Volcanic Province and Region Surrounding the Northern Lake Malawi Rift Basin, Master's Thesis, The Pennsylvania State University.

Bowman, J. R., and M. Ando (1987), Shear-wave splitting in the upper-mantle wedge above the Tonga subduction zone, *Geophys. J. Int.*, 88(1), 25-41, doi: 10.1111/j.1365-246X.1987.tb01367.x.

Bram, K., and B. Schmeling (1975), Structure of crust and upper mantle beneath the Western Rift of East Africa, derived from investigations of near earthquakes: Afar between continental and oceanic rifting, 138-142.

Castaing, C., (1991), Post-Pan-African tectonic evolution of South Malawi in relation to the Karroo and recent East African rift systems, *Tectonophysics*, 191(1-2), 55-73.

Chakrabarti, R., A. R. Basu, A. P. Santo, D. Tedesco, and O. Vaselli (2009), Isotopic and geochemical evidence for a heterogeneous mantle plume origin of the Virunga volcanics, Western rift, East African Rift system, *Chemical Geology*, 259(3–4), 273-289.

Conrad, C.P., and M.D. Behn (2010), Constraints on lithosphere net rotation and asthenospheric viscosity from global mantle flow models and seismic anisotropy, *Geochemistry, Geophysics, Geosystems*, 11(5).

Currie, C.A. and van Wijk, J. (2016). How craton margins are preserved: Insights from geodynamic models. *Journal of Geodynamics*, *100*, pp.144-158.

Delvaux, D., and A. Barth (2010), African stress pattern from formal inversion of focal mechanism data, *Tectonophysics*, 482(1), 105-128.

De Waele, B., J.P. Liégeois, A.A. Nemchin, and F. Tembo (2006), Isotopic and geochemical evidence of Proterozoic episodic crustal reworking within the Irumide Belt of south-central Africa, the southern metacratonic boundary of an Archaean Bangweulu Craton, *Precambrian Res.*, 148(3), 225-256.

Ebinger, C. J., and N. H. Sleep (1998), Cenozoic magmatism throughout east Africa resulting from impact of a single plume, *Nature*, 395(6704), 788-791.

Ebinger, C. J., A. L. Deino, R. E. Drake, and A. L. Tesha (1989), Chronology of volcanism and rift basin propagation: Rungwe Volcanic Province, East Africa, *J. Geophys. Res.*, 94(B11), 15785–15803, doi:10.1029/JB094iB11p15785.

Ebinger, C. J., G. D. Karner, and J. K. Weissel (1991), Mechanical strength of extended continental lithosphere: constraints from the western rift system, East Africa, *Tectonics*, 10(6), 1239-1256.

Eilon, Z., G. A. Abers, G. Jin, and J. B. Gaherty (2014), Anisotropy beneath a highly extended continental rift, *Geochemistry, Geophysics, Geosystems*, 15(3), 545-564.

Fernandez-Alonso, M., and K. Theunissen (1998), Airborne geophysics and geochemistry provide new insights in the intracontinental evolution of the Mesoproterozoic Kibaran belt (Central Africa), Geological Magazine, 135(02), 203-216.

Fishwick, S., and I. D. Bastow (2011), Towards a better understanding of African topography: a review of passive-source seismic studies of the African crust and upper mantle, *Geological Society, London, Special Publications*, 357(1), 343-371.

Fontijn, K., Williamson, D., Mbede, E. and Ernst, G.G. (2012), The Rungwe Volcanic Province, Tanzania–A volcanological review. *Journal of African Earth Sciences*, *63*, pp.12-31.

Fritz, H., M. Abdelsalam, K.A. Ali, B. Bingen, A.S. Collins, A.R. Fowler, W. Ghebreab, C.A. Hauzenberger, P.R. Johnson, T.M. Kusky, and P. Macey (2013), Orogen styles in the East African Orogen: a review of the Neoproterozoic to Cambrian tectonic evolution, *Journal of African Earth Sciences*, 86, 65-106.

Gao, S., P. M. Davis, H. Liu, P. D. Slack, A. W. Rigor, Y. A. Zorin, V. V. Mordvinova, V. M. Kozhevnikov, and N. A. Logatchev (1997), SKS splitting beneath continental rift zones, J. Geophys. Res., 102(B10), 22781–22797, doi:10.1029/97JB01858.

Gripp, A.E., and R.G. Gordon (2002), Young tracks of hotspots and current plate velocities,*Geophysical Journal International*, 150(2), 321-361.

Hammond, J.O.S., and J.M. Kendall (2016), Constraints on melt distribution from seismology: a case study in Ethiopia, *Geological Society, London, Special Publications*, 420(1), 127-147.

Hansen, L. N., Y.H. Zhao, M.E. Zimmerman, and D.L. Kohlstedt (2014), Protracted fabric evolution in olivine: Implications for the relationship among strain, crystallographic fabric, and seismic anisotropy,*Earth and Planetary Science Letters*, 387, 157-168.

Hansen, S. E., A. A. Nyblade, and M. H. Benoit (2012), Mantle structure beneath Africa and Arabia from adaptively parameterized P-wave tomography: Implications for the origin of Cenozoic Afro-Arabian tectonism, *Earth and Planetary Science Letters*, *319*, 23-34, doi:10.1016/j.epsl.2011.12.023.

Hilbert-Wolf, H. L., E. M. Roberts, and E. L. Simpson (2016), New sedimentary structures in seismites from SW Tanzania: Evaluating gas-vs. water-escape mechanisms of soft-sediment deformation, *Sedimentary Geology*, 344, 253-262.

Hodgson, I., F. Illsley-Kemp, D. Keir, C. J. Ebinger, K. Mtelela (2017), Magmatic activity at a young continental rift: A receiver function study from the Tanganyika rift, in Gu, J., editor, Special Issue of Tectonics.

Holtzman, B. K., and J.-M. Kendall (2010), Organized melt, seismic anisotropy, and plate boundary lubrication, *Geochem. Geophys. Geosyst.*, 11, Q0AB06, doi:10.1029/2010GC003296.

Homuth, B., U. Löbl, A. G. Batte, K. Link, C.M. Kasereka, and G. Rümpker (2016), Seismic anisotropy of the lithosphere/asthenosphere system beneath the Rwenzori region of the Albertine Rift. *International Journal of Earth Sciences*, 105(6), 1681-1692.

Kampunzu, A.B., P. Akanyang, R.B.M. Mapeo,, B.N. Modie, and M. Wendorff (1998), Geochemistry and tectonic significance of the Mesoproterozoic Kgwebe metavolcanic rocks in northwest Botswana: implications for the evolution of the Kibaran Namaqua-Natal belt, *Geological Magazine*, 135(5), 669-683.

Kaneshima, S., M. Ando, and S. Kimura (1988), Evidence from shear-wave splitting for the restriction of seismic anisotropy to the upper crust, *Nature*, 335, 627-629.

Keir, D., M. Belachew, C.J. Ebinger, J.M. Kendall, J.O.S. Hammond, G.W. Stuart, A. Ayele, and J.V. Rowland (2011), Mapping the evolving strain field during continental breakup from crustal anisotropy in the Afar Depression, *Nature Communications*, *2*, 285, doi:10.1038/ncomms1287.

Kendall, J.M., and C. Lithgow-Bertelloni, (2016), Why is Africa rifting?, *Geological Society, London, Special Publications*, 420(1), 11-30.

Kendall, J. M., S. Pilidou, D. Keir, I. D. Bastow, G. W. Stuart, and A. Ayele (2006), Mantle upwellings, melt migration and the rifting of Africa: insights from seismic anisotropy, in *The Afar Volcanic Province within the East African Rift System*, edited by G. Yirgu, C. J. Ebinger, and P. K. H. Maguire, Geological Society, London, Special Publications, 259, 55-72.

King, S. D., and D. L. Anderson (1998), Edge-driven convection, *Earth and Planetary Science Letters*, 160(3), 289-296.

Liu, K.H., and S.S. Gao (2013), Making reliable shear-wave splitting measurements, Bull. Seismol. Soc. Am.,103, 2680–2693, doi:10.1785/0120120355.

Lynner, C., and M. D. Long (2014), Lowermost mantle anisotropy and deformation along the boundary of the African LLSVP, *Geophys. Res. Lett.*, 41, 3447–3454, doi:10.1002/2014GL059875.

Mardia, K. V. (1975), Statistics of directional data (with discussion), *J. R. Stat. Soc. B*, 37, 349–393.

Mavonga, T., S. K. Kavotha, N. Lukaya, O. Etoy, W. Mifundu, R. K. Bizimungu, and J. Durieux (2010), Some aspect of seismicity prior to the 27 November 2006 eruption of Nyamuragira volcano and its implication for volcano monitoring and risk mitigation in the Virunga area, Western Rift Valley of Africa, *J. of African Earth Sciences*, 58(5), 829-832.

McCartney, T., and C. A. Scholz (2016), A 1.3 million year record of synchronous faulting in the hangingwall and border fault of a half-graben in the Malawi (Nyasa) Rift, *Journal of Structural Geology*, 91, 114-129.

McConnell, R. B. (1967), The east African rift system, *Nature*, 215, 578-581.

Mesko, G. T., C. Class, M. D. Maqway, N. Boniface, S. Manya, and S. R. Hemming (2014, December), The Timing of Early Magmatism and Extension in the Southern East African Rift: Tracking Geochemical Source Variability with 40Ar/39Ar Geochronology at the Rungwe Volcanic Province, SW Tanzania, In *AGU Fall Meeting Abstracts*, 1, 4730.

Montagner, J.-P. (1994), Can seismology tell us anything about convection in the mantle?, *Rev. Geophys.*, 32(2), 115–137, doi:10.1029/94RG00099.

Morley, C. K., S. M. Cunningham, R. M. Harper, and W. A. Wescott (1992), Geology and geophysics of the Rukwa rift, East Africa, *Tectonics*, 11(1), 69-81.

Mortimer, E., D. A. Paton, C. A. Scholz, M. R. Strecker, and P. Blisniuk, (2007), Orthogonal to oblique rifting: effect of rift basin orientation in the evolution of the North basin, Malawi Rift, East Africa, *Basin Research*, 19(3), 393-407.

Mulibo, G. D., and A. A. Nyblade (2013), Mantle transition zone thinning beneath eastern Africa: Evidence for a whole-mantle superplume structure, *Geophys. Res. Lett.*, 40, 3562–3566, doi:10.1002/grl.50694.

Ni, S., E. Tan, M. Gurnis, and D. Helmberger (2002), Sharp sides to the African superplume, *Science*, 296(5574), 1850-1852, doi: 10.1126/science.1070698.

Nicolas, A. and N. I. Christensen (1987), Formation of Anisotropy in Upper Mantle Peridotites - A Review, in *Composition, Structure and Dynamics of the Lithosphere-Asthenosphere System*, edited by K. Fuchs and C. Froidevaux, American Geophysical Union, Washington, D. C.. doi: 10.1029/GD016p0111.

Nyblade, A. A., and S. W. Robinson (1994), The African superswell, *Geophysical Research Letters*, 21(9), 765-768, doi:10.1029/94GL00631.

O'Donnell, J. P., A. Adams, A. A. Nyblade, G. D. Mulibo, and F. Tugume (2013), The uppermost mantle shear wave velocity structure of eastern Africa from Rayleigh wave

tomography: constraints on rift evolution, *Geophys. J. Int.*, 194(2), 961-978, doi: 10.1093/gji/ggt135.

Rasskazov, S.V., N.A. Logachev, A.V. Ivanov, A.A. Boven, M.N. Maslovskaya, E.V. Saranina, I.S. Brandt and S.B. Brandt, (2003), A magmatic episode in the western rift of East Africa (19-17 ma), *Geologiya i Geofizika*, 44(4), 317-324.

Reed, C. A., K. H. Liu, Y. Yu, and S. S. Gao (2017), Seismic anisotropy and mantle dynamics beneath the Malawi Rift Zone, East Africa, *Tectonics*, 36, 1338–1351, doi:10.1002/2017TC004519.

Restivo, A., and G. Helffrich (1999), Teleseismic shear wave splitting measurements in noisy environments, *Geophys. J. Int.*, 137(3), 821-830.

Ring, U. (1994), The influence of preexisting structure on the evolution of the Cenozoic Malawi rift (East African rift system), *Tectonics*, 13(2), 313-326.

Ritsema, J., A. A. Nyblade, T. J. Owens, C. A. Langston, and J. C. VanDecar (1998), Upper mantle seismic velocity structure beneath Tanzania, east Africa: Implications for the stability of cratonic lithosphere, *J. Geophys. Res.*, 103(B9), 21201–21213, doi:10.1029/98JB01274.

Roberts, E.M., N.J. Stevens, P.M. O'Connor, P.H.G.M. Dirks, M.D. Gottfried, W.C. Clyde, R.A. Armstrong, A.I.S. Kemp, and S. Hemming (2012), Initiation of the western branch of the East African Rift coeval with the eastern branch, *Nature Geo.*, 5(4), 289-294, doi:10.1038/ngeo1432.

Rosendahl, B. R., E. Kilembe, and K. Kaczmarick (1992), Comparison of the Tanganyika, Malawi, Rukwa and Turkana Rift zones from analyses of seismic reflection data, *Tectonophysics*, 213(1), 235-256.

Saltzer, R.L., J.B. Gaherty, and T.H. Jordan (2000), How are vertical shear wave splitting measurements affected by variations in the orientation of azimuthal anisotropy with depth?, *Geophysical Journal International*, 141(2), 374-390.

Saria, E., E. Calais, D.S. Stamps, D. Delvaux, and C.J.H. Hartnady (2014), Present- day kinematics of the East African Rift, *Journal of Geophysical Research: Solid Earth*, 119(4), 3584-3600.

Savage, M. K. (1999), Seismic anisotropy and mantle deformation: What have we learned from shear wave splitting?, *Rev. Geophys.*, 37(1), 65–106, doi:10.1029/98RG02075.

Shillington, D.J., J.B. Gaherty, C.J. Ebinger, C.A. Scholz, K. Selway, A.A. Nyblade, P.A. Bedrosian, C. Class, S. L. Nooner, M. E. Pritchard, J. Elliott, P. R. N. Chindandali, G. Mbogoni, R. W. Ferdinand, N. Boniface, S. Manya, G. Kamihanda, E. Saria, Gabriel Mulibo, J. Salima, A. Mruma, L. Kalindekafe, N.J. Accardo, D. Ntambila, M. Kachingwe, G.T. Mesko, T. McCartney, M. Maquay, J. P. O'Donnell, G. Tepp, K.Mtelela, P. Trinhammer, D. Wood, E. Aaron, M. Gibaud, M. Rapa, C. Pfeifer, F. Mphepo, D. Gondwe, G. Arroyo, C. Eddy, B. Kamoga, and M. Moshi (2016), Acquisition of a unique onshore/offshore geophysical and geochemical dataset in the northern Malawi (Nyasa) Rift, *Seis. Res. Lett*., 87(5), doi:10.1785/0220160112.

Silver, P. G., and W. W. Chan (1991), Shear wave splitting and subcontinental mantle deformation, *J. Geophys. Res.*, 96(B10), 16429–16454, doi:10.1029/91JB00899.

Silver, P. G., S. S. Gao, K. H. Liu, and the Kaapvaal Seismic Group (2001), Mantle deformation beneath southern Africa, Geophys. Res. Lett., 28, 2493-2496.

Sleep, N. H., C. J. Ebinger and J.-M. Kendall (2002), Deflection of mantle plume material by cratonic keels, Geological Society, London, Special Publications, 199, 135-150.

Smets, B., D. Delvaux, K.A. Ross, S. Poppe, M. Kervyn, N. d'Oreye, and F. Kervyn, (2016), The role of inherited crustal structures and magmatism in the development of rift segments: Insights from the Kivu basin, western branch of the East African Rift, *Tectonophysics*, 683, 62-76.

Tommasi, A., M. Knoll, A. Vauchez, J. W. Signorelli, C. Thoraval, and R. Logé (2009), Structural reactivation in plate tectonics controlled by olivine crystal anisotropy, *Nature Geoscience*, 2(6), 423-427.

Van der Beek, P., E. Mbede, P. Andriessen, and D. Delvaux (1998), Denudation history of the Malawi and Rukwa Rift flanks (East African Rift System) from apatite fission track thermochronology, *Journal of African Earth Sciences*, 26(3), 363-385.

Versfelt, J., and B. R. Rosendahl (1989), Relationships between pre-rift structure and rift architecture in Lakes Tanganyika and Malawi, East Africa, *Nature*, 337, 354-357.

Walker, K. T., A. A. Nyblade, S. L. Klemperer, G. H. R. Bokelmann, and T. J. Owens (2004), On the relationship between extension and anisotropy: Constraints from shear wave splitting across the East African Plateau, *J. Geophys. Res.*, 109, B08302, doi:10.1029/2003JB002866.

Wauthier, C., V. Cayol, F. Kervyn, and N. d'Oreye (2012), Magma sources involved in the 2002 Nyiragongo eruption, as inferred from an InSAR analysis, *Journal of Geophysical Research: Solid Earth*, 117(B5).

Weeraratne, D. S., D. W. Forsyth, K. M. Fischer, and A. A. Nyblade (2003), Evidence for an upper mantle plume beneath the Tanzanian craton from Rayleigh wave tomography, *J. Geophys. Res.*, 108, 2427, doi:10.1029/2002JB002273.

Wölbern, I., G. Rümpker, K. Link, and F. Sodoudi (2012), Melt infiltration of the lower lithosphere beneath the Tanzania craton and the Albertine rift inferred from S receiver functions, *Geochemistry, Geophysics, Geosystems*, 13(8).

Wood, D. A., H. J. Zal, C. A. Scholz, C. J. Ebinger, and I. Nizere, (2017), Evolution of the Kivu Rift, East Africa: Interplay among tectonics, sedimentation and magmatism, *Basin Research*, 29(S1), 175-188.

Wookey, J., J. M. Kendall, and G. Rümpker (2005), Lowermost mantle anisotropy beneath the north Pacific from differential S-ScS splitting, *Geophys. J. Int.*, 161(3), 829-838, doi: 10.1111/j.1365-246X.2005.02623.x.

Wüstefeld, A., G. Bokelmann, C. Zaroli, and G. Barruol (2008), SplitLab: A shear-wave splitting environment in Matlab, *Computers & Geosciences*, 34(5), 515-528, doi:10.1016/j.cageo.2007.08.002.

Yu, Y., S. S. Gao, M. Moidaki, C. A. Reed, and K. H. Liu (2015), Seismic anisotropy beneath the incipient Okavango rift: Implications for rifting initiation, *Earth and Planetary Science Letters*, *430*, 1-8, doi:10.1016/j.epsl.2015.08.009.

Table 1. Measurement Parameters and Errors by Array

Array		Total Measurements	Average measurements per station (range)	RC Method	
		SKS SKKS		SNR > 8	SNR > 4
SeGMENT		456 172	7.6 (2-17) 2.9 (0-9)	248 (54%) 56 (33%)	438 (96%) 167 (97%)
	Land-based	*444* *155*	*8.1 (2-17)* *2.8 (0-9)*	*246 (55%)* *53 (34%)*	*427 (96%)* *150 (97%)*
	Lake-bottom (LBS)	*12* *17*	*2.4 (2-4)* *3.4 (1-6)*	*2 (17%)* *3 (18%)*	*11 (92%)* *17 (100%)*
TANGA14		192 119	14.8 (5-27) 9.2 (2-21)	114 (59%) 50 (42%)	180 (94%) 108 (91%)
Kivu		36 14	7.2 (1-17) 2.8 (0-6)	6 (17%) 5 (36%)	31 (86%) 11 (79%)
Total		684 305	8.8 (1-27) 3.9 (0-21)	368 (54%) 111 (36%)	649 (95%) 286 (94%)

Table 1. continued

SC Method		RC Method		SC Method	
SNR > 8	SNR > 4	Average ϕ 2σ error	Average δt 2σ error (sec)	Average ϕ 2σ error	Average δt 2σ error (sec)
302 (66%) 85 (49%)	449 (98%) 172 (100%)	19.1° 21.0°	0.35 0.44	23.0° 25.5°	0.60 0.66
297 (67%) 77 (50%)	438 (99%) 155 (100%)	18.5° 19.9°	0.32 0.43	23.1° 25.6°	0.58 0.65
5 (42%) 8 (47%)	11 (92%) 17 (100%)	25.5° 28.5°	0.61 0.50	21.8° 25.1°	0.82 0.66
139 (72%) 70 (59%)	190 (99%) 116 (97%)	21.3° 23.1°	0.39 0.63	27.2° 27.4°	0.72 0.96
15 (42%) 6 (43%)	35 (97%) 13 (93%)	17.5° 23.9°	0.42 0.57	18.1° 14.5°	0.68 0.75
456 (67%) 161 (53%)	674 (99%) 301 (99%)	19.4° 21.7°	0.36 0.49	23.5° 25.1°	0.63 0.73

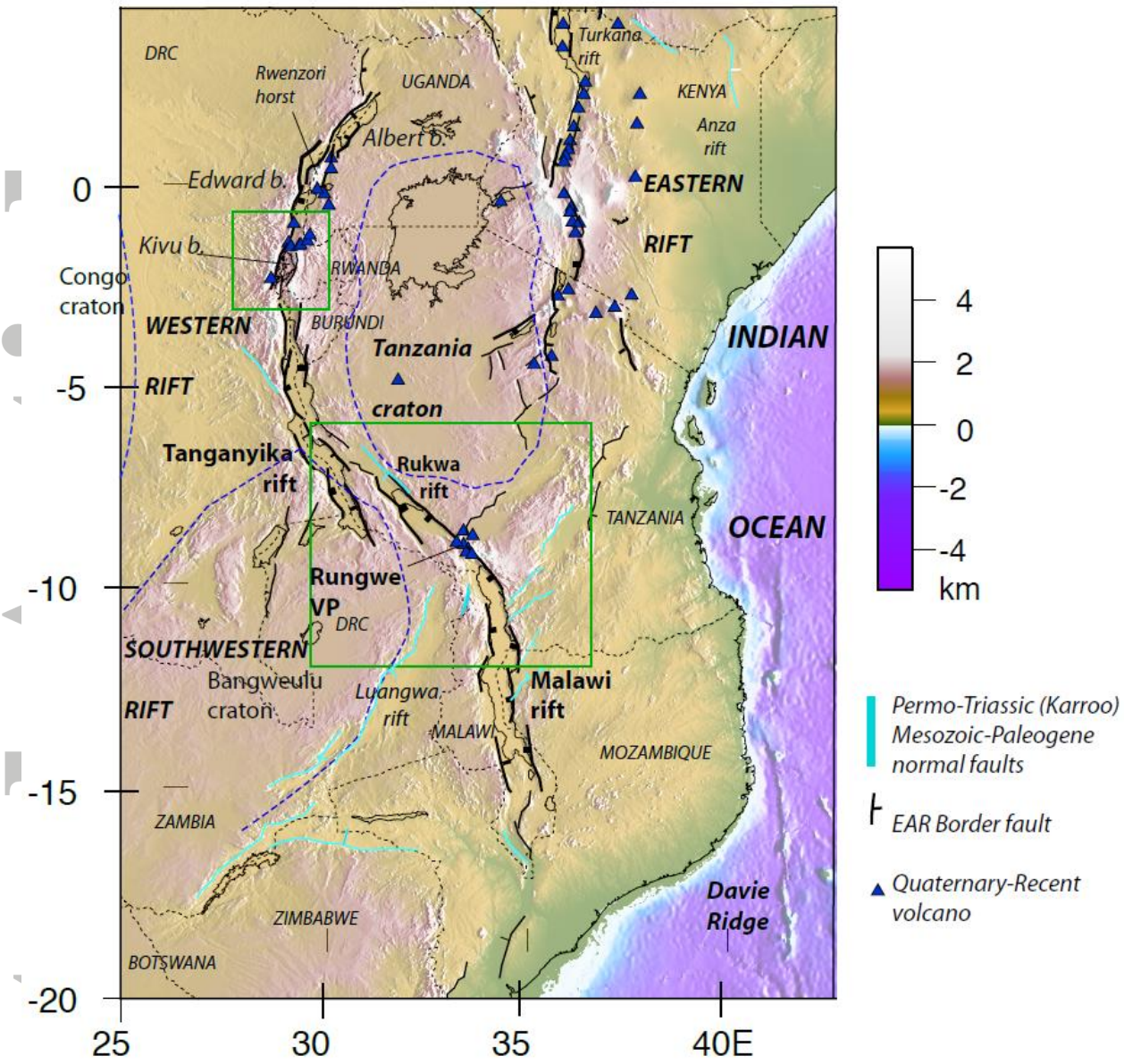

Figure 1. Major border faults and Quaternary eruptive centers of the East African rift system with respect to Permo-Triassic (Karroo) rift systems with respect to thick Archaean cratons enclosed by dashed blue lines. The green boxes enclose the Tanganyika-Rukwa- Malawi and Kivu study areas shown in subsequent figures. After Ebinger and Scholz [2012].

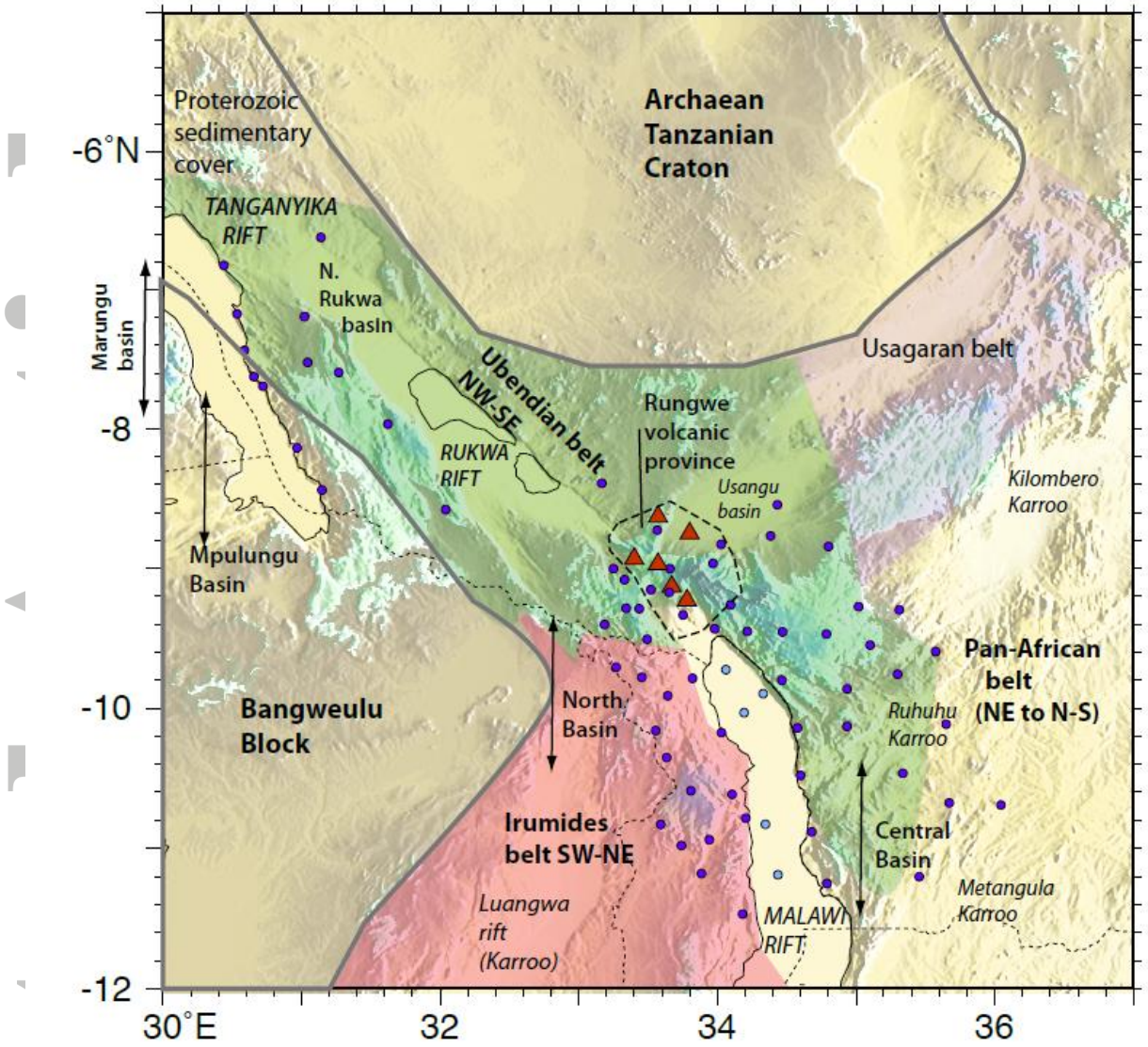

Figure 2. Map of seismic stations relative to fault bounded rift basins and major tectonic units in the Tanganyika-Rukwa-Malawi rift zone. Bangweulu Block = Paleoproterozoic craton; Ubendian belt = Paleoproterozoic orogenic belt; Irumides belt = Mesoproterozoic orogenic belt; Pan-African = crust reworked in Neoproterozoic [after Fritz et al., 2013]. Karroo rifts are Permo-Triassic, and small outcrops of Cretaceous-Palaeogene sequences are not shown [e.g., Roberts et al., 2012]. Circles denote temporary seismic stations (purple) and lake-bottom seismometers (cyan) used in this study. Red triangles denote the Quaternary volcanoes within the Rungwe volcanic province. Solid lines outline the large lakes within the rift valleys.

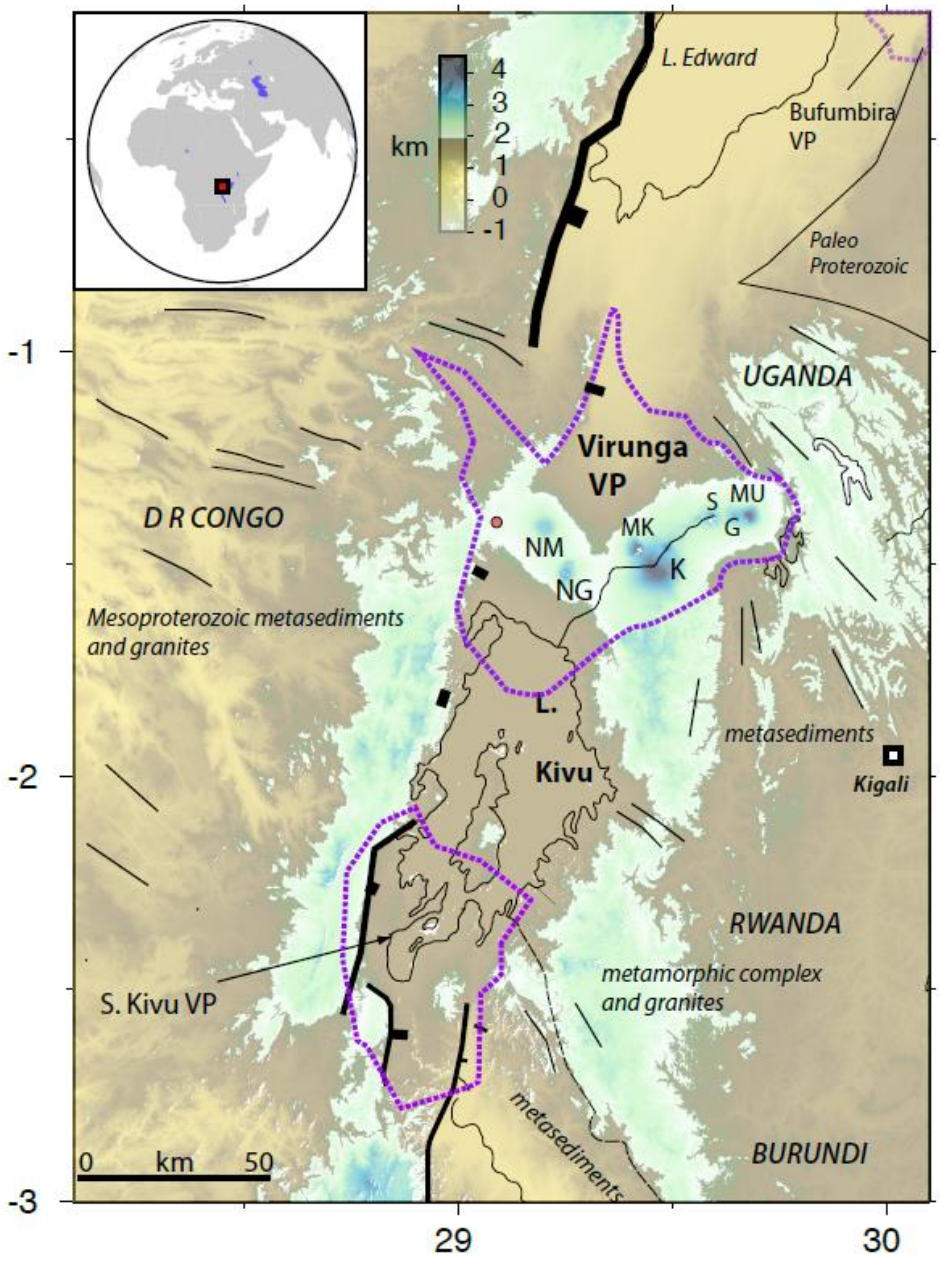

Figure 3. Location of KIVU12 seismometers and geological summary of the Kivu rift region with bold lines showing border faults and with light lines indicating dominant orientation of metamorphic fabric [after Wood et al., 2017]. Dashed lines enclose surface expression of Miocene-Recent magmatism (Bufumbira, Virunga, S. Kivu provinces). Volcanoes within the Virunga volcanic province (VVP) are labeled. The blue regions on the inset map are large lakes.

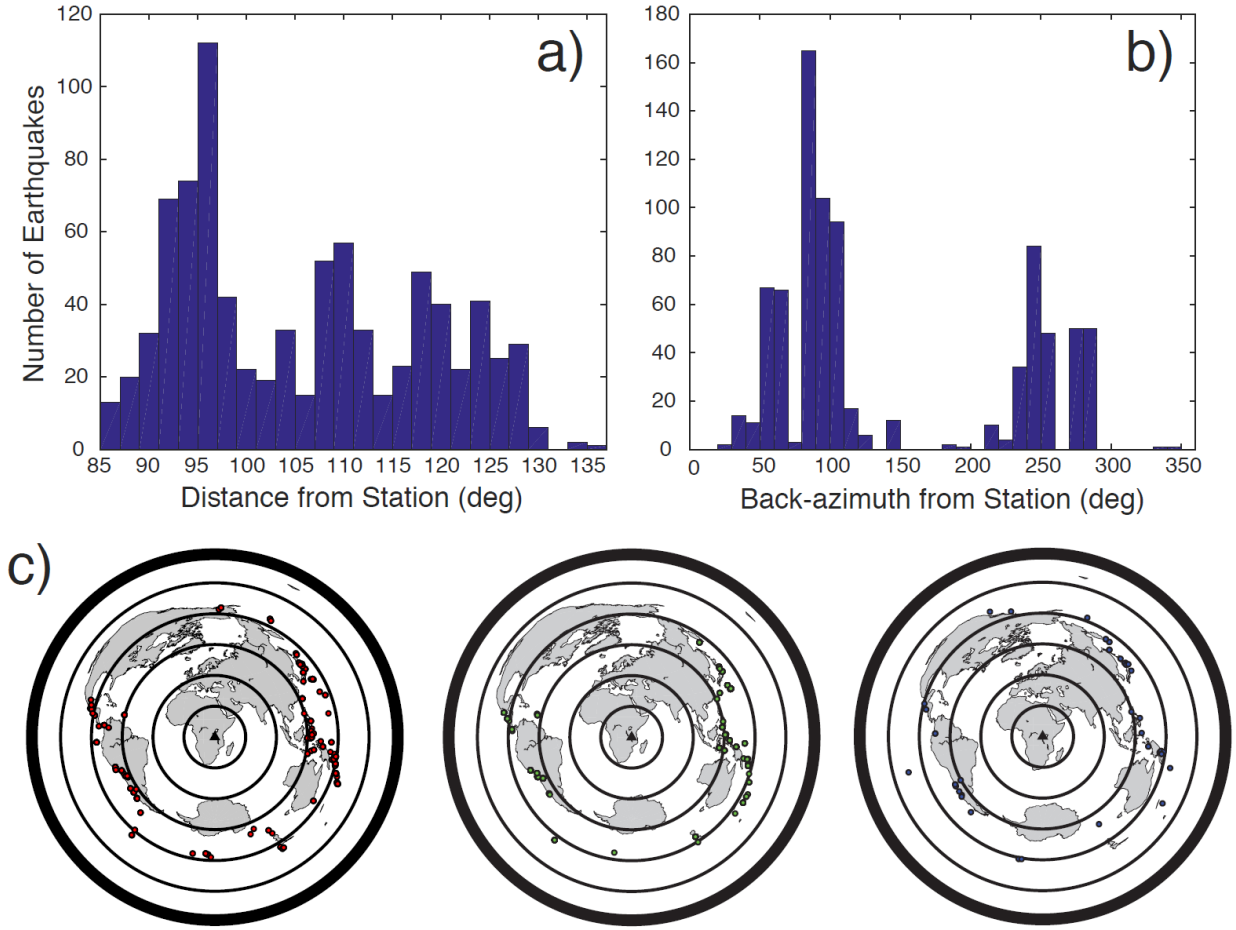

Figure 4. Histograms of the (a) angular distances and (b) back-azimuths for all earthquake-station pairs measured in this study. Bin widths are 2º for distances and 10º for back-azimuths. Back-azimuth is measured clockwise from N. (c) Maps of the earthquakes used for each array: SEGMeNT (left, red), TANGA14 (center, green), and KIVU12 (right, blue).

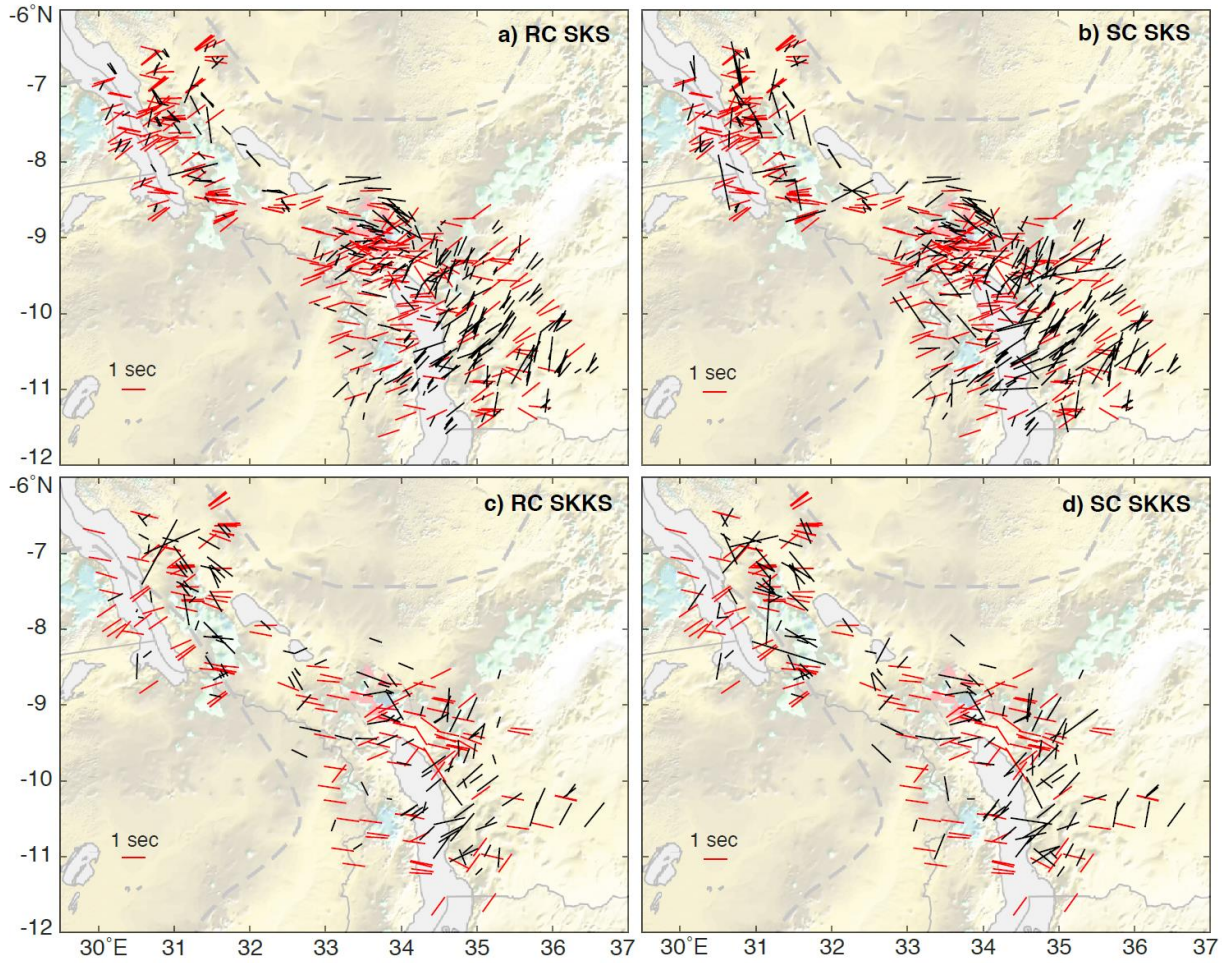

Figure 5. All anisotropy measurements of the SEGMeNT and TANGA14 arrays: SKS using the (a) RC and (b) SC method and SKKS using the (c) RC and (d) SC method. All lines are centered on the rays' 210-km pierce points. See Figure S8 for a plot with lines at the rays' 100-km pierce points. Black lines indicate a measured fast splitting direction with length proportional to delay time. Red lines indicate a null measurement (see section 4) with the angle equivalent to the back-azimuth (assumed polarization direction) and a fixed length (1 sec).

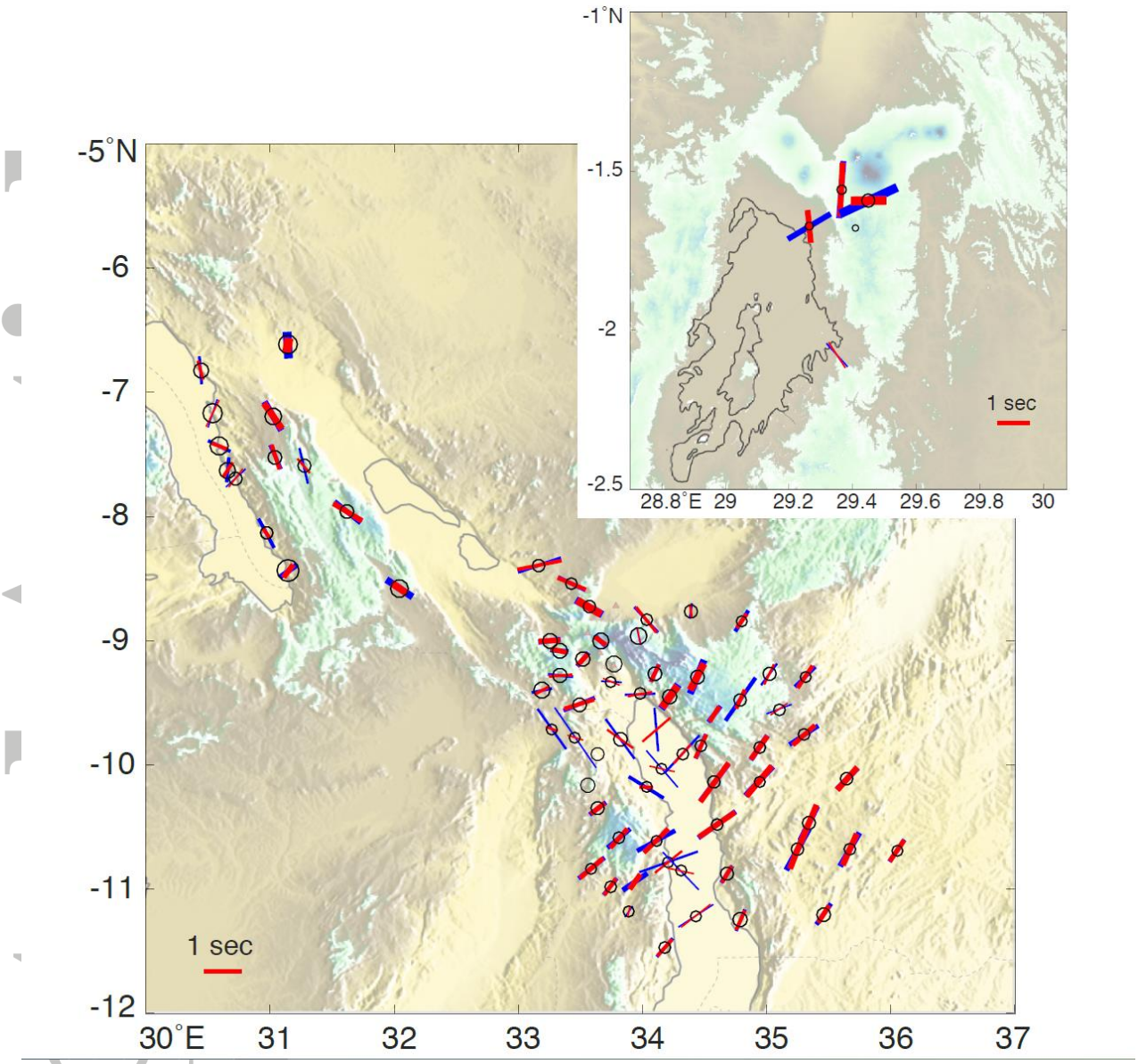

Figure 6. Station averaged SKS splitting directions in the Tanganyika-Rukwa-Malawi rift zone (main) and Kivu rift (inset): Lines indicate the weighted average fast splitting direction for the SC method (blue) and the RC method (red). Line length is proportional to the weighted average delay time. Line thickness is proportional to the number of non-null measurements, with thicker lines having more measurements. Null measurements are indicated by the open black circles, whose radius is scaled by the number of null measurements at the station.

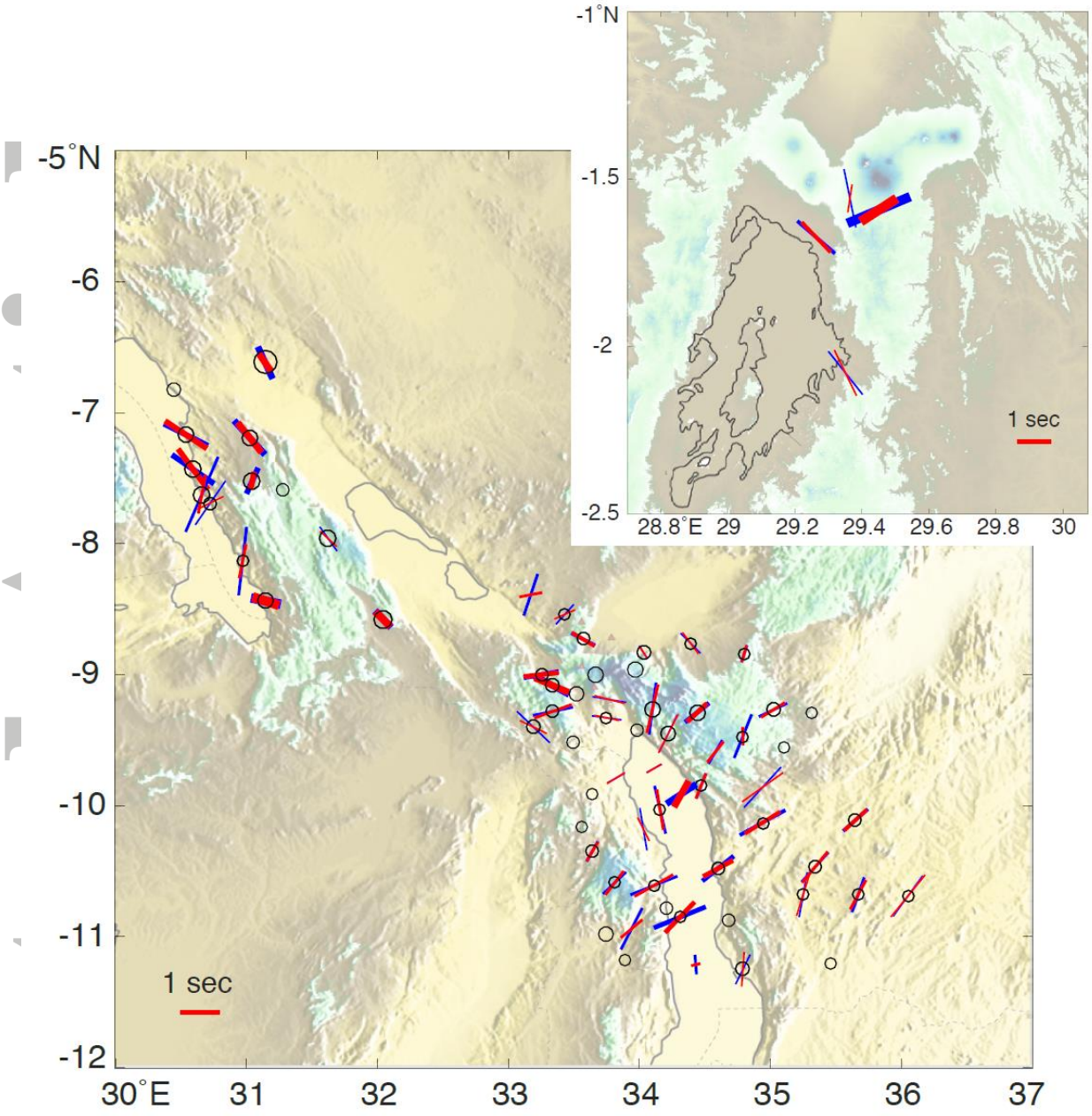

Figure 7. Station averaged SKKS splitting directions. Lines indicate the weighted average fast splitting direction for the SC method (blue) and the RC method (red). Line length is proportional to the weighted average delay time. Line thickness is proportional to the number of non-null measurements, with thicker lines having more measurements. Null measurements are indicated by the open black circles, scaled by the number of null measurements at the station.

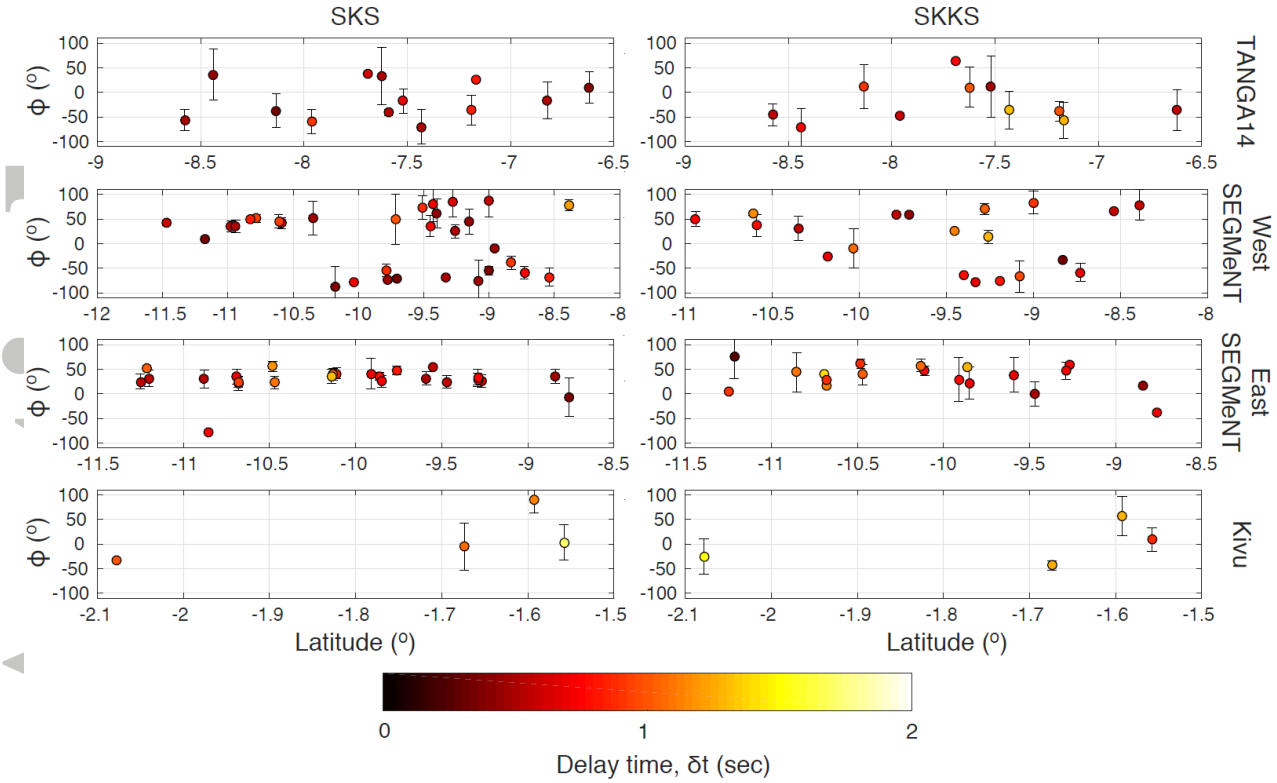

Figure 8. N-S splitting direction trends of RC SKS and SKKS for each array. The SEGMeNT array is split into east and west using the 34.3°E longitude line, approximately the Malawi rift axis. Color is delay time, δt, in seconds. Error bars show weighted standard deviation. No error bars indicates a single measurement at the station.

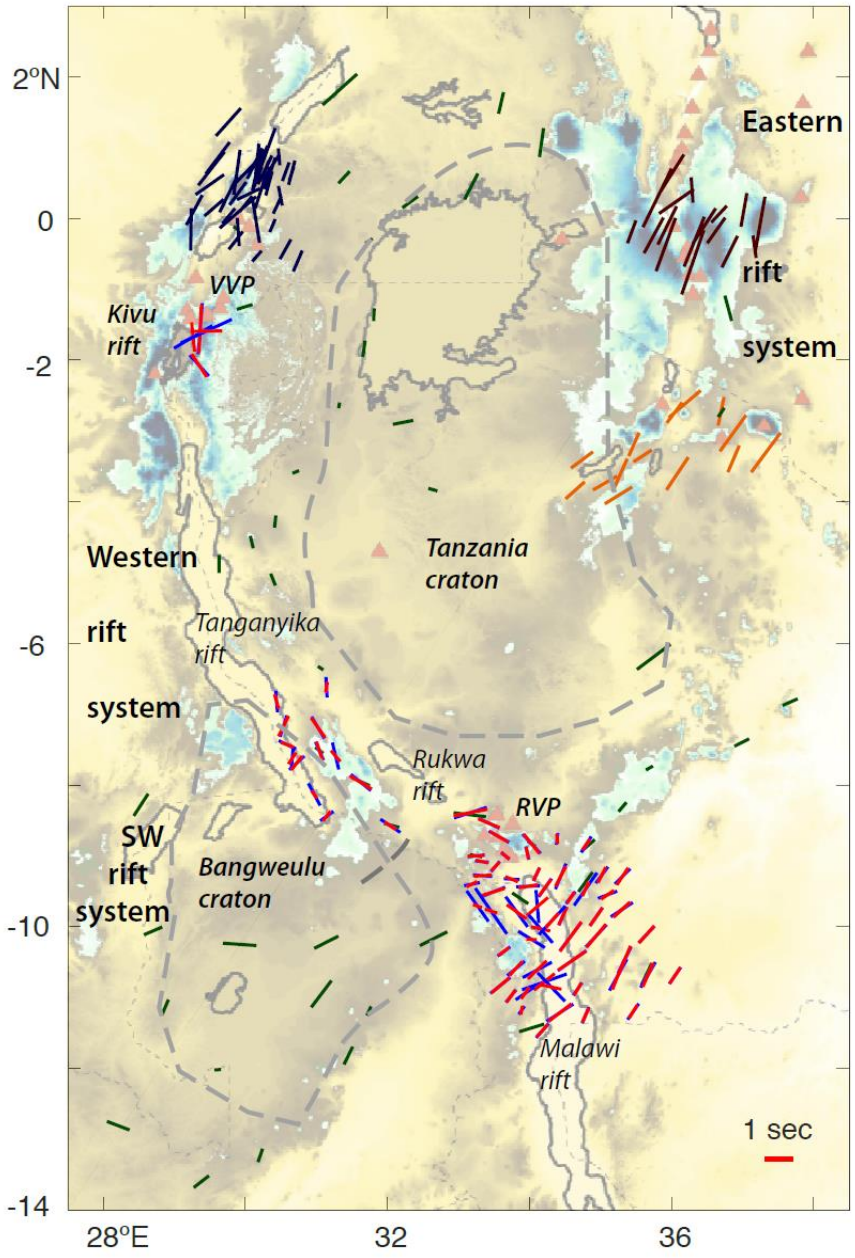

Figure 9. Comparison of SKS splitting results with other studies. Blue and red lines denote SC and RC methods, respectively, from this study. Other lines denote splitting results from Gao et al. [1997] (dark red), Bagley and Nyblade [2013] (green), Albaric et al. [2014] (yellow), and Homuth et al. [2016] (dark blue). Line length is proportional to the weighted average delay time for this study and the published delay time for the other studies. Red triangles mark volcanoes. Shorelines of lakes are outlined.

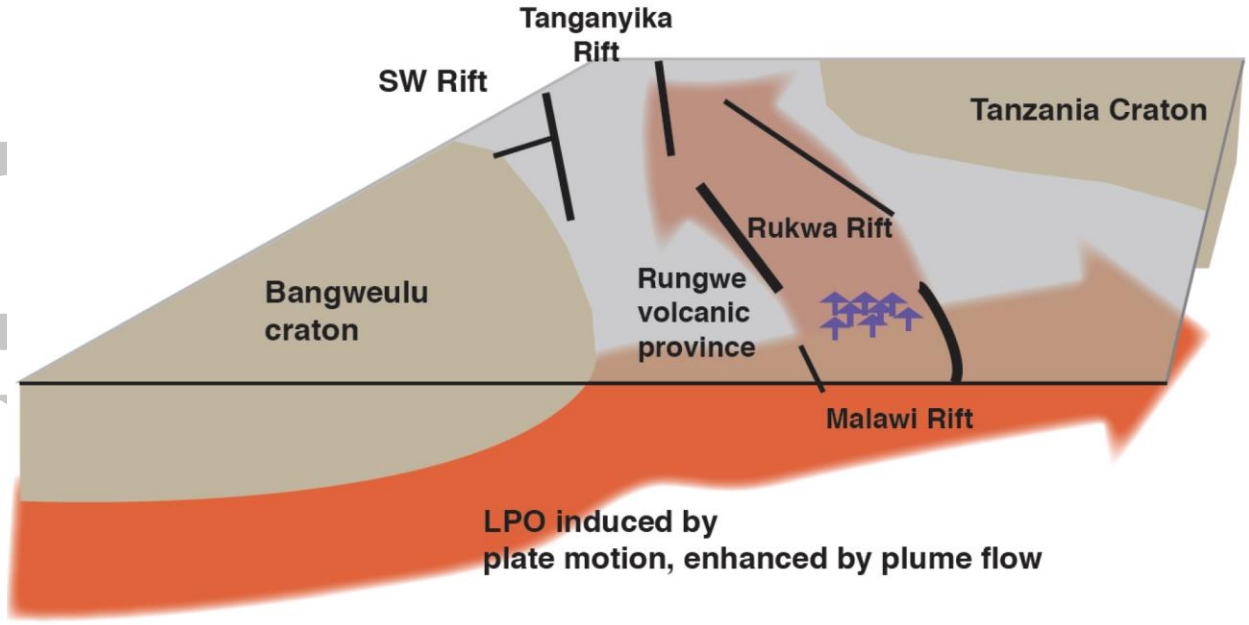

Figure 10. Schematic diagram of mantle flow and anisotropy beneath the study area. The large red arrows represent the mantle flow direction from plate motion. The orange arrows show the deflection of mantle flow around the Bangweulu and Tanzania cratons. Rifts are shown by dashed lines.